Unique interpretation of Talbot Bands and Fourier domain white light interferometry

Adrian Gh. Podoleanu

School of Physical Sciences, University of Kent, Canterbury, CT2 7NH, UK

ap11@kent.ac.uk

Abstract: A theoretical model is developed to interpret the output of the diffraction grating spectrometer used to analyze the channelled spectrum produced by a low coherence interferometer set-up. This model leads to an unique interpretation which covers both cases (i) of Talbot bands and (ii) of a Michelson interferometer used in most spectral interferometry set-ups for sensing as well as for Fourier domain optical coherence tomography (FDOCT). Explanation of Talbot bands visibility as well as the decay of sensitivity with depth, characteristic for FDOCT, is explained by considering the extension of the two wavetrains diffracted by the diffraction grating in the spectrometer.

OCIS Codes: (120.3180) Interferometry; (120.6200) Spectrometers and spectroscopic instrumentation; (110.4500) Optical Coherence Tomography.

References and links

1. L. M. Smith, C. C. Dobson, "Absolute Displacement Measurements using Modulation of the Spectrum of White Light in a Michelson Interferometer," Appl. Opt. **28**, 3339-42, (1981).
2. J. Schwider and Liang Zhou, "Dispersive interferometric profilometer," **19,** Opt. Lett. 995-997, 1994).
3. K. -N. Joo and S. -W. Kim, "Absolute distance measurement by dispersive interferometry using a femtosecond pulse laser," Opt. Express **14**, 5954-5960 (2006)
4. S. Taplin, A. Gh. Podoleanu D. J. Webb, D. A. Jackson, "Displacement Sensor Using Channeled Spectrum Dispersed on a Linear CCD Array," Electron. Lett. **29,** 896-897, (1993).
5. A. Gh. Podoleanu S. Taplin,D. J. Webb, D. A. Jackson, "Channelled Spectrum Liquid Refractometer," Rev. Sci. Instr. **64,** 3028-9, (1993).
6. G. Hausler, M. W. Lindner, ""Coherence radar" and "spectral radar" – new tools for dermatological diagnosis," J. Biomed. Opt. **3,** 21-31 (1998).
7. R. Leitgeb, C. K. Hitzenberger, and A. F. Fercher, "Performance of Fourier domain vs. time domain optical coherence tomography", Opt. Express **11**, 889-894, (2003).
8. J. F. de Boer, B. Cense, B. H. Park, M. C. Pierce, G. J. Tearney, and B. E. Bouma, "Improved signal-to-noise ratio in spectral-domain compared with time-domain optical coherence tomography," Opt. Lett. **28,** 2067-2069 (2003).
9. T. Endo, Y. Yasuno, S. Makita, M. Itoh, and T. Yatagai, "Profilometry with line-field Fourier-domain interferometry," Opt. Express **13**, 695-701 (2005).
10. B. Park, M. C. Pierce, B. Cense, S. -H. Yun, M. Mujat, G. Tearney, B. Bouma, and J. de Boer, "Real-time fiber-based multi-functional spectral-domain optical coherence tomography at 1.3 µm," Opt. Express **13**, 3931-3944 (2005)
11. A. Gh. Podoleanu, S. TaplinD. J. Webb, D. A. Jackson, "Channeled Spectrum Display using a CCD Array for Student Laboratory Demonstrations," European J. Phys. **15,** 266-271, (1994).
12. F. A. Jenkins, H. E. White, in Fundamentals of Optics, (McGraw-Hill, 1957), 284;
13. M. Wojtkowski, R. Leitgeb, A. Kowalczyk, T. Bajraszewski, A. F. Fercher ,"In vivo human retinal imaging by Fourier domain optical coherence tomography," J. Biomed. Opt. 7, 457-463 (2002).
14. A. Bachmann, R. Leitgeb, and T. Lasser, "Heterodyne Fourier domain optical coherence tomography for full range probing with high axial resolution," Opt. Express **14**, 1487-1496 (2006)
15. M. A. Choma, M. V. Sarunic, C. Yang and J. A. Izatt, "Sensitivity advantage of swept source and Fourier domain optical coherence tomography," Opt. Express **11**, 2183-2189, (2003).
16. A. B. Vakhtin, K. A. Peterson, and D. J. Kane, "Resolving the complex conjugate ambiguity in Fourier-domain OCT by harmonic lock-in detection of the spectral interferogram," Opt. Lett. **31**, 1271-1273 (2006).
17. M. Sarunic, M. A. Choma, C. Yang, and J. A. Izatt, "Instantaneous complex conjugate resolved spectral domain and swept-source OCT using 3x3 fiber couplers," Opt. Express **13**, 957-967 (2005).

#81518 - $15.00 USD Received 29 Mar 2007; revised 17 Jul 2007; accepted 18 Jul 2007; published 20 Jul 2007

18. F. Talbot, “An experiment on the interference of light,” Philos. Mag. **10**, 364, (1837).
19. G. B. Airy, “The Bakerian Lecture – on the theoretical explanation of an apparent new polarity of light,” Phil. Trans. R. Soc. London **130**, 225-244, (1840).
20. A. L. King and R. Davis, “The Curious Bands of Talbot,” Am. J. Phys. **39**, 1195-1198, (1971).
21. A. Gh. Podoleanu, S. Taplin, D. J. Webb, D. A. Jackson, "Talbot-like Bands for Laser Diode Below Threshold," J. Opt. A, Pure Appl. Opt. **6**, 413 - 424, (1997).
22. A. Gh. Podoleanu, S. Taplin, D. J. Webb and D. A. Jackson, "Theoretical Study of Talbot-like Bands Observed Using a Laser Diode Below Threshold," J. Opt. A, Pure Appl. Opt. Vol. 7, (1998), 517-536.
23. M. Warengham, C. P. Grover, “Dispersion curve measurement using Talbot bands,” Revue Phys. Appl. **23**, 1169-1178 (1998).
24. M. Wojtkowski, A. Kowalczyk, R. Leitgeb, and A. F. Fercher, "Full range complex spectral optical coherence tomography technique in eye imaging," Opt. Lett. **27,** 1415-1417 (2002).

1. Introduction

Spectral domain white light interferometry (SDWLI) has been increasingly used for optical sensing purposes [1-5] as well as in optical coherence tomography (OCT). In the last five years, considerable research has been devoted to Fourier domain optical coherence tomography (FDOCT) for tissue imaging [6-10]. FDOCT or spectral radar is a form of spectral domain white light interferometry. SDWLI and FDOCT refer to Fourier transformation of the photodetected signal delivered by a spectrometer at the output of a low coherence interferometer [11]. The spectrum exhibits peaks and troughs in the form of a channelled spectrum [12] and the frequency of such a modulation is proportional to the modulus of the optical path difference (OPD) in the interferometer. FDOCT is attractive because eliminates the need for depth scanning which in time domain OCT is usually performed by mechanical means.

However, in SDWLI and FDOCT, the same result is obtained for positive and negative OPDs, a problem which could be addressed by the method proposed here, inspired from Talbot bands. In FDOCT, to avoid the superposition of images of opposite OPD sign, the OPD=0 position is initially adjusted outside the range of interest. This is not possible all the time, especially when imaging moving organs or tissue. Different methods inspired from phase shifting interferometry can be used to eliminate the mirror terms [13-16] and attenuate one of the image. A truly fused 3x3 coupler having an even power splitting ratio between the ports exhibits 120^0 phase difference between the outputs [17]. These can be conveniently used to generate quadrature components to eliminate the mirror terms. However, this method introduces attenuation, and although better suited for moving objects, relies on exact values of phase shifts. Therefore such method requires calibration of parameters, whose values have to be exact within a given bandwidth and have also to be stable in time.

All methods mentioned above work on cancellation of the mirror terms, which when not perfect for different reasons, allows the mirror terms to reappear. These methods increase the acquisition time and therefore are sensitive to movement.

2. Talbot bands

Talbot bands represent a curious effect, discovered by Talbot in 1837 [18]. When a glass plate is introduced halfway into the beam coming from a white light source, modulation of the spectrum in the form of a channeled spectrum (CS) or Talbot bands appear only when the glass plate intercepts a certain side of the beam. G. B. Airy [19] dispelled any “curious” effects as mere results of interference which enhances the amplitude of some wavelengths and reduces the amplitude of others. When using a prism, the plate should be introduced into the side corresponding to the red part [20] of the dispersed spectrum while when using a diffraction grating, the plate should be introduced into the blue side of the beam. So far, the optical configurations producing Talbot bands and those using a Michelson interferometer in

#81518 - $15.00 USD Received 29 Mar 2007; revised 17 Jul 2007; accepted 18 Jul 2007; published 20 Jul 2007

most sensing and OCT systems have been dealt with independently. In this paper I propose a unique model to explain the CS for both types of experiments.

A CS is observed using the bulk implementation shown in Fig. 1, where the optical beam from a broadband optical source, BOS, is collimated by a lens L1, and directed towards a beamsplitter BS. The light received by the beamsplitter BS is split into a sensing or object beam, OB, along the object path leading to an object mirror OM and into a reference beam, RB, along a reference path leading to a reference mirror RM. (In OCT applications, the object arm includes a transverse scanner and the OM is replaced by tissue or a multi-layer structure). The resulting beam from the BS is then sent to a diffraction grating, (or a prism) where the spectrum is diffracted to an output fan of rays with different wavelengths, subsequently focused by a focusing element L2 onto a photodetector array or a CCD linear array [1-11]. The CCD driver converts this spatial distribution into a temporal distribution. Using an electrical spectrum analyzer, ESA, the frequency of the channelled spectrum modulation is determined which leads to the |OPD| value. If multi-layered objects are imaged, such as tissue, each layer imprints its own CS periodicity, depending on its |OPD|.

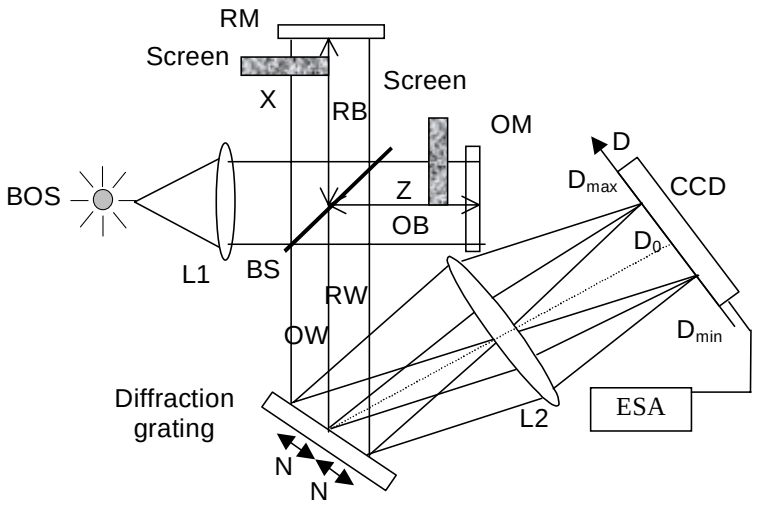

Fig. 1. Modified Michelson interferometer configuration [21] to reproduce Talbot bands and distinguish between positive and negative OPDs.

In a previous report [21] we demonstrated that a modified Michelson configuration can be used for studying the Talbot bands. By introducing screens in the Michelson interferometer, as shown in Fig. 1, the CS obtained when using a laser diode below threshold as a low coherence source was simplified. In these reports we have shown that the CS contains components due to the combination of the OPD in the interferometer with the OPD equivalent to the laser cavity length [22]. The simplification of the FFT spectrum of the CS is intimately related to the process of elimination of Talbot bands, as described in this paper. With a configuration as that in Fig. 1 with screens, CS bands are visible for one sign of the OPD only and there is an optimum OPD where the visibility is maximum. These particularities are characteristics of Talbot bands. Although Talbot bands represent an old known effect, there was no attempt in using Talbot bands to eliminate the mirror terms in FDOCT so far, despite the considerable attention to FDOCT in the last 5 years. In the following, I explain how Talbot bands could be used for selection in OPD sign and elimination of mirror terms. I present a theoretical model which covers Talbot bands, SDWLI and FDOCT set-ups.

#81518 - $15.00 USD Received 29 Mar 2007; revised 17 Jul 2007; accepted 18 Jul 2007; published 20 Jul 2007

3. Theoretical model

Based on the theoretical model in [22] and the system in Fig. 1, I obtain a unique equation for the photodetector CCD current covering both cases, of screens-in and no-screens. In addition to the notation and the case dealt with in [22], I introduce a parameter q, where q = 1 for screens-in and q = 2 for no-screens.

After the screens in Fig. 1 are introduced halfway through, the remaining optical waves are denoted as object wave, OW and reference wave, RW. The field diffracted at an angle θ can be written as superposition of these two waves diffracted:

$$V(\theta,\bar{\lambda},t)=\frac{1}{\sqrt{2}}\{Z_O(\theta,\bar{\lambda})O(\bar{\lambda})X(\bar{\lambda},t)+\exp[j2\pi(2-q)pND\bar{\lambda}]Z_R(\theta,\bar{\lambda})R(\bar{\lambda})X(\bar{\lambda},t)\} \quad (1)$$

where $\bar{\lambda}$ is the wavenumber, t is the time, D is the differential delay between rays diffracted by two adjacent grating lines and $X(\bar{\lambda},t)=Y(\bar{\lambda})\exp[-j2\pi ct\bar{\lambda}]$ is the source optical field, with c the speed of light in the interferometer space. O and R describe the action of region of refractive index perturbation along the object and reference arms in the interferometer respectively and Z_O, Z_R describe the effect of the diffraction grating, considered as being uniformly illuminated within the transverse section of the two beams. When no screens are in place, $Z_O = Z_R$ and both terms involve qN grating lines, with q=2. When the screens are in place, then Z_O and Z_R involve different sets of grating lines. If the screens are introduced halfway through into the two beams, then the number of lines intercepted is qN, with q=1.

Essential for what follows is that an "intrinsic" delay between the two waves OW and RW is introduced by the diffraction grating. This is described by the phase term in the second term in Eq. (1) when 2-q = 1. This is the consequence of the delay between the 1st ray in the diffracted beam of RW in relation to the 1st ray in the diffracted beam of OW. This is due to the Bragg condition, as from diffracted ray on each slit to the next, the wave encounters a delay:

$$D=a(\sin\theta_i-\sin\theta)=p\lambda \quad (2)$$

which for N grating lines is $pN\lambda$, where p is an integer and signifies the diffraction order. The angles θ_i and θ of the incident and diffracted rays are measured from the diffraction grating normal to the reflected and diffracted rays and a is the grating spacing. Later on, we will restrict the discussion to the first order of diffraction, $p=\pm1$, where the choice of sign depends on the grating orientation relative to the direction of incoming beams.

Considering the transmission along the two object and reference beams described by T_O and T_R respectively and that the delays along the object optical path is t_O and along the reference optical path is t_R:

$$O(\bar{\lambda})X(\bar{\lambda},t)=T_OY(\bar{\lambda})\exp[-j2\pi c(t-t_O)\bar{\lambda}] \quad (3a)$$

and

$$R(\bar{\lambda})X(\bar{\lambda},t)=T_RY(\bar{\lambda})\exp[-j2\pi c(t-t_R)\bar{\lambda}] \quad (3b)$$

with

$$\Delta t=t_O-t_R \quad (3c)$$

the temporal delay introduced by the interferometer and the OPD = $c\Delta t$.

Starting with an equation similar to (1), reference [22] presents a detailed evaluation of the CCD photocurrent during one read time sequence as result of the interference of two diffracted waves. Following the same steps as in reference [22], a more complete equation for the CCD photocurrent is obtained including the effect of the phase factor depending on q in (1). For brevity, similar assumptions are considered, such as the negligible effect of pixelation when each CCD pixel is a lot smaller than the size of the diffracted spot determined by the

#81518 - $15.00 USD Received 29 Mar 2007; revised 17 Jul 2007; accepted 18 Jul 2007; published 20 Jul 2007

grating resolution, that the photodetector responsivity is η and that the source spectrum profile $|Y(\bar{\Lambda})|^2$ in the wavenumber space $\bar{\Lambda}$ is a Gaussian centered around the wavenumber $\bar{\lambda}_0$ in the middle of the spectrum:

$$|Y(\bar{\Lambda})|^2 = \frac{1}{\sqrt{2\pi\sigma}} \exp[-\frac{(\bar{\Lambda} - \bar{\lambda}_0)^2}{2\sigma^2}] \tag{4a}$$

where the coefficient σ is related to the FWHM of the line-width in wavelength, $\Delta\lambda$ by:

$$\sigma = \frac{\Delta\lambda}{2\sqrt{2\ln 2}\bar{\lambda}_0^2} \tag{4b}$$

Then, the amplitude autocorrelation function, g(x), of the optical field generated by the source is also a Gaussian, according to the equation:

$$F\{|Y(\bar{\Lambda})|^2\} = g(x)\exp(i2\pi\bar{\lambda}_0 x) \tag{4c}$$

where F signifies the Fourier transformation from the wavenumber space $\bar{\Lambda}$ to a space described by coordinate x and

$$g(x) = \exp(-2\pi\sigma^2 x^2) \tag{4d}$$

Introducing the notation:

$$\psi(x) = g(x)\cos(2\pi\bar{\lambda}_0 x) \tag{5}$$

and following the same steps as in the Appendix A in reference [22], the CCD photocurrent results as:

$$I(D) = \eta\frac{1}{2qN}(T_O^2 + T_R^2)\sum_{s=-(qN-1)}^{qN-1} C_s\{\psi(sD) + \frac{2T_O T_R}{T_O^2 + T_R^2}\psi[(s + p(2-q)N)D - c\Delta t]\} \tag{6}$$

For an axis D oriented along the CCD array, D will be considered positive, with values between D_{min} and D_{max} spectrum edges (Fig. 1) sampled by the CCD. The sign of the phase term in Eq. (1) depends on the grating orientation and is incorporated into p. Summing the diffracted rays from all grating lines, it can be shown that the coefficients C_s are given by:

$$C_s = qN - |s| \tag{7a}$$

for

$$-qN + 1 \le s \le qN - 1 \tag{7b}$$

The first term in Eq. (6) describes the spectrum profile of the optical source sampled by the CCD length. The second term represents modulation of the spectrum, i.e. the CS.

Different visibility profiles of the CS versus the optical path difference, $c\Delta t$, in the interferometer are obtained, depending on the case, screens-in or out. The amplitude autocorrelation function varies quickly with its argument for a low coherent source, the larger the source bandwidth, the narrower the g(x) profile. Therefore, the most relevant terms contributing to the CS in Eq. (6), for a given OPD value, are those with zero or small argument of the correlation function g. Argument zero for g happens when:

$$c\Delta t = sD + p(2-q)ND \tag{8}$$

When this is combined with Eq. (7b), it gives the range of OPD within which a CS is produced. Depending on the sign in the exponential of the second term in Eq. (1), which depends on the sign of p in Eq. (2), the range of OPD is:

#81518 - $15.00 USD Received 29 Mar 2007; revised 17 Jul 2007; accepted 18 Jul 2007; published 20 Jul 2007

$$[2(1-q)N+1]D \le c\Delta t \le (2N-1)D \quad \text{for } p=1 \tag{9a}$$

and

$$-(2N-1)D \le c\Delta t \le -[2(1-q)N+1]D \quad \text{for } p=-1 \tag{9b}$$

For q=2, the case with no screens, both equations (9) give the same range for OPD:

$$(-2N+1)D \le c\Delta t \le (2N-1)D \tag{10a}$$

However, when the screens are in, q=1, depending on the orientation of the grating, i.e. on the sign of the phase factor in the second term in Eq. (1), Eq. (9a) and Eq. (9b) give respectively:

$$D \le c\Delta t \le (2N-1)D \quad \text{for } p=1 \tag{10b}$$

and

$$-(2N-1)D \le c\Delta t \le -D \quad \text{for } p=-1 \tag{10c}$$

The set-up with no screens (equivalent to set-ups largely used in sensing and in all FDOCT reports) produces a CS for positive and negative OPD values as predicted by Eq. (10a). The case with screens-in (Talbot bands), produces a CS for positive OPD values only, according to Eq. (10b) and for negative OPD values only, according to Eq. (10c), depending on the grating tilt (the sign of p) in relation to the incoming beam direction.

3.1. Visibility decay with OPD

An approximate evaluation of the visibility of the CS can be performed as follows. If the source spectrum is sufficiently wide, then the amplitude correlation function g defined in Eq. (4d) decays rapidly with its argument which includes the OPD. Therefore, a limited number of terms, $2r \approx 2\frac{\lambda_0}{\Delta\lambda}$ in Eq. (6) present significant values. For this limited number of terms, and for $c\Delta t >> l_c$ (coherence length of the optical source), the cosines in the second terms in Eq. (6) can be approximated as pulsating with the same periodicity. Let us denote the point closest to the center of the spectrum $D_0 = \lambda_0$ by D_m, then Eq. (8) is satisfied for the index s taking the particular value:

$$S_m = \mathrm{Int}(c\Delta t / D_m) - p(2-q)N \tag{11}$$

where Int(α) means the integer value of the argument α. Considering small variations δD_m about the point D_m, the visibility of the CS is then given by :

$$V_q \approx \frac{2T_O T_R}{T_O^2 + T_R^2} \frac{\sum_{s=S_m-r}^{S_m+r} C_s g[(s - S_m)D_m]}{\sum_{s=-r}^{r} C_s g(sD_m)} \tag{12}$$

Using Eq. (7a), Eq. (12) becomes:

$$V_q \approx \frac{2T_O T_R}{T_O^2 + T_R^2} \frac{(qN-|S_m|)[g(0) + 2\sum_{\varepsilon=1}^{r} g(\varepsilon D_m)]}{qNg(0) + 2\sum_{\varepsilon=1}^{r}[(qN-\varepsilon)g(\varepsilon D_m)]} \tag{13}$$

In practice, N>>r, which leads to further simplification of Eq. (13) to:

$$V_q \approx \frac{2T_O T_R}{T_O^2 + T_R^2} \frac{qN-|S_m|}{qN} \tag{14}$$

#81518 - $15.00 USD Received 29 Mar 2007; revised 17 Jul 2007; accepted 18 Jul 2007; published 20 Jul 2007

Equation (14) describes a triangular shape of the visibility with maximum for $S_m = 0$ for both cases, screen-in or out. For screens-in, this represents the known triangular profile for Talbot bands [23]. However, the triangular profile is obtained for different OPD ranges in the two cases, either symmetric around OPD=0 according to Eq. (10a) or covering one OPD sign only, according to Eq. (10b) or Eq. (10c). The decay of visibility with OPD for systems like in Fig. 1 with no screens (q=2), was discussed in previous papers on sensing and FDOCT in the context of spectrometer resolution [6,13]. I will show here that the decay is mere the result of the same phenomenon which could be used to explain the decay of sensitivity with the OPD in a Talbot bands like experiment.

3.2 Heuristic explanation of sensitivity decay with OPD

A simple explanation can be put forward based on the fact that the coherence length of the dispersed wave by a prism or of the diffracted wave by a diffraction grating is longer than the coherence length of the incoming wave. This particularity can be used to explain the Talbot bands and extended to explain selection in the OPD values of the configuration in Fig. 1 with or without screens. In this respect, let us consider a temporal view of the partial coherence light as made of femtosecond pulses. Each diffraction grating slit generates a replica of the incoming pulse (wavelet) in the first order of diffraction, delayed by λ. For example, for a superluminiscent diode at $1\ \mu m$, of several tens of nm linewidth, the coherence length is in the range of $10\ \mu m$. Using 2N=2000 grating lines (no screens in Fig. 1) means a wavetrain length of 2N individual pulses (wavelets) of $10\ \mu m$ length each, delayed in between by $1\ \mu m$. As consequence, the total wavetrain is as long as 2 mm. Table 1 shows the superposition of diffracted wavetrains for different values of OPDs for the two cases, screens-out (top raw) and screens-in (2^{nd} and 3^{rd} raw). The assumption is that the grating is on the left and the wavetrains travel to the CCD array to the right of each sketch. R and L signify wavetrains produced by the right, respectively left side of the grating. Wavetrains for N = 6 grating lines are shown for simplicity.

The 6 pulses in the wavetrains mark the spatial position of the maximum of each wavelet diffracted, and are shown narrower than the space between them, λ, for simplicity, to illustrate in a small sketch the dependence between the wavetrain length and the number of diffraction lines intercepted. (In fact, each wavelet extends for more than several wavelengths either side for most real cases of several micron coherence length sources and may be wider than the length of the whole wavetrain for 6 pulses only, however when a large number of pulses are considered, the wavetrain length is practically proportional to the number of diffracted wavelets in the wavetrain with a good approximation. Also, as it will be understood later from interpreting the Table 1, the temporal extension of each wavelet has insignificant effects on the channelled spectrum visibility versus OPD when N is large).

The striking difference between the two cases is due to the existence or not of the "intrinsic" delay in Eq. (1) introduced by the dispersion element (here the diffraction grating). No 'intrinsic' delay means that the two wavetrains are totally superposed, as shown in the top raw of Table 1. When the OPD goes higher (positive or negative), the two wavetrains emerging from the diffraction grating are delayed in relation to each other and the amount of overlap reduces, as shown for OPD = $\pm N\lambda$ and becomes zero for OPD= $\pm 2N\lambda$, observing the triangular profile dependence on OPD as described by Eq. (14). For q=1 the behaviour is different, in OPD = 0 there is no overlap due to the existence of the 'intrinsic' delay, so no CS modulation. Therefore, the two wavetrains can be superposed only by introducing a definite sign of OPD in the interferometer. Let us define the OPD as the difference between the object

#81518 - $15.00 USD Received 29 Mar 2007; revised 17 Jul 2007; accepted 18 Jul 2007; published 20 Jul 2007

Table 1. Overlap of the two wavetrains versus OPD.

$c\Delta t$	$-2N\lambda$	$-N\lambda$	0	$N\lambda$	$2N\lambda$
Case 2 No screens q=2 SDWLI and FDOCT	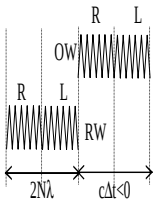	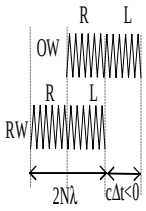	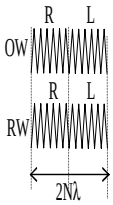	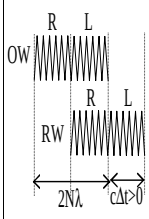	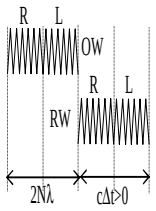
	Zero overlap	Partial overlap	Maximum overlap	Partial overlap	Zero overlap
Case 1 Screens in place q=1, p=1 Talbot bands	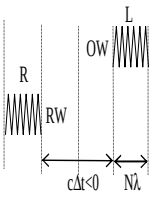	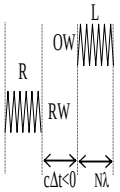	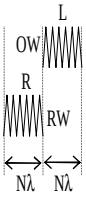	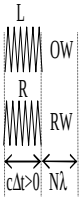	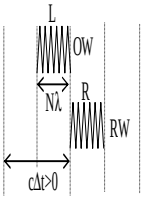
	No overlap	No overlap	Zero overlap	Maximum overlap	Zero overlap
Case 1 Screens in place q=1, p=-1 Talbot bands	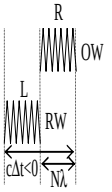	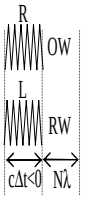	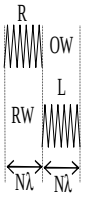	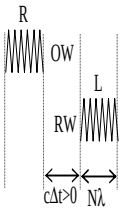	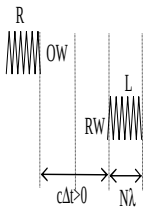
	Zero overlap	Maximum overlap	Zero overlap	No overlap	No overlap

path length, and the reference path length, according to (3c): OPD=2Z-2X, where distances X and Z are shown in Fig 1.In the second raw, p=1 signifies such an 'intrinsic' delay of the reference wavetrain RW in relation to the object wavetrain OW, that for OPD = 0, RW lags behind OW. In the third raw, the orientation of the grating is such that the 'intrinsic' delay makes OW lag behind RW. For p=1, delaying the object wave (2nd raw) and for p = -1, delaying the reference wave (3rd raw) allows overlap of the two wavetrains to take place. As consequence, with the screens-in, starting from zero OPD, the visibility of the CS can be made either to increase or stay at zero value, in opposition to the case of no-screens where the visibility decays with OPD either side of OPD = 0.

In the following I show that the sketches of the wavetrains in Table 1 are in accordance to the theoretical model developed above. The different ranges of OPD values determined by (10a,b,c) are inferable from Table 1 by considering the amount of overlap of the two wavetrains. In the top raw, positive and negative OPD values lead to overlap of the waves and so to a CS. The ambiguity created by what is called mirror terms in FDOCT is illustrated by the cases of $OPD = \pm N\lambda$ which exhibit similar overlap. In the other two raws the ambiguity is eliminated, negative OPD values in the 2nd raw and positive OPD values in the 3rd raw increase the separation of the two wavetrains, so no overlap and therefore a CS is obtained for one sign of OPD only.

#81518 - $15.00 USD Received 29 Mar 2007; revised 17 Jul 2007; accepted 18 Jul 2007; published 20 Jul 2007

At an OPD value, of $c\Delta t = 2N\lambda$ (last column), the overlap is brought to zero and the visibility of the CS rolls-off to zero. This is in accordance with Eq. (10a) (first raw) and Eq. (10b) (second raw). The same is valid for the first column, according to Eq. (10a) (first raw) and Eq. (10c) (third raw). These give the maximum OPD measurable values in SDWLI sensing set-ups and in FDOCT.

The interpretation here for the maximum OPD range, derived from the study of Talbot bands is more fundamental than that invoking the spectrometer resolution [6,13] and provides an explanation based on the length and relative delay of the wavetrains after the diffraction grating, delay represented as a combination of the `intrinsic` delay due to dispersion (diffraction) with that introduced in the interferometer. The combination of the two delays is described by Eq. (8). In fact, the interferometer arms are extended up to the CCD array including the spectrometer. With no screens, the OPD reduces to the genuine optical path difference evaluated up to the beamsplitter. With the screens-in, this genuine OPD is combined with the 'intrinsic' delay.

Also, the OPD values where maximum visibility is predicted by the theoretical model above are obtainable by evaluating the overlap for the three cases in Table 1. The visibility registers a maximum for $S_m = 0$ in Eq. (14). For q = 2, Eq. (11) leads to $c\Delta t = 0$ (however no CS exists until the |OPD| is at least comparable with the coherence length of the source). In table 1, top raw, the two wavetrains OW and RW have a spatial length of $2N\lambda$ and for OPD = 0 are totally superposed. For q=1, according to (11), the value $S_m = 0$ is obtained for $c\Delta t = +ND_m \approx +N\lambda_0$ for p = 1 and $c\Delta t = -ND_m \approx -N\lambda_0$ for p = -1. The same values are obtained from the 2nd and 3rd raws, where the two wavetrains OW and RW have a spatial length of $N\lambda$ and are totally superposed for $OPD = N\lambda$ in the 2nd raw and for $OPD = -N\lambda$ in the 3rd raw. In addition to selection in the OPD sign, this method moves the OPD value of maximum visibility towards the middle of the range. This property is important in OCT, where it could be advantageously used to compensate for the attenuation of signal with depth in the tissue.

4. Conclusions

I derived a theoretical model which provides an equation applicable to both cases of screens-in (Talbot bands) and no-screens (case valid for all reports on FDOCT) in Fig. 1. A supplementary explanation of differences in behavior of the system with the screens-in and screens-out is provided by considering the equivalent length of the wavetrains after the diffraction grating. This allows a simple heuristic interpretation of the Talbot bands generation and extension of similar principles to applications requiring operation for one sign of OPD only. The paper shows that: (i) the same Eq. (6), Eq. (11) and Eq. (14) can be put forward to explain the CS properties in a wide range of interferometers; (ii) based on the extension of coherence length of the diffracted waves due to diffraction, the variation of the CS strength with OPD can be explained. The Eq. (11) and Eq. (14) were then validated against the heuristic interpretation represented in Table 1, based on the extension of the diffracted wavetrains and shown delayed by the 'intrinisic delay'. The model (Eq. (6) and Eq. (14) and interpretation in Table 1) is applicable to both cases of Talbot bands as well as to Michelson configurations with spectral interrogation. This interpretation is fruitful in showing that the later case could be interpreted as superposition of wavetrains in configurations producing Talbot bands (superposition of wavetrains in raws 2 and 3 gives the wavetrains in raw 1).

An important conclusion is that by modifying an FDOCT interferometer to produce Talbot bands, is possible to sense the sign of the OPD in the interferometer. This could be employed in sensing as well as to eliminate the mirror terms in FDOCT and advantageously shift the visibility maximum towards the middle of the OPD range.

Such a method is superior to all other known methods to resolve the ambiguity in the OPD sign, all based on cancellation techniques inspired from phase shifting interferometry [13,14] or complex Fourier signal processing [16], methods which require calculations which take time and also well adjusted and stable parameters. Therefore, the method proposed is less

#81518 - $15.00 USD Received 29 Mar 2007; revised 17 Jul 2007; accepted 18 Jul 2007; published 20 Jul 2007

sensitive to experimental set-up adjustment and does not require combination of signals and computation, simply the system is made sensitive to one sign of the optical path difference (OPD) only.

It is however true that based on Talbot bands the range is not doubled like in complex Fourier OCT set-ups, which tolerate the OPD=0 crossing the useful range. However the attenuation of mirror terms using Talbot bands is superior to any other methods proposed because it is not based on cancellation procedures.

The explanation put forward here does not deny the assertion in previous FDOCT papers that the spectrometer resolution is responsible for the sensitivity decay with OPD. The spectrometer resolution depends on the number of grating lines, N, and according to Table 1, the overlap of the two wavetrains is reduced to zero when the OPD is longer than $N\lambda$. However, the explanation here shows the fundamental origin of the decay of sensitivity with OPD. Other factors limiting the spectrometer resolution such as the number of photodetectors in the array interrogating the spectrum should be considered in addition to the phenomenon explained in Table 1, of signal decay due to the reduction of overlap of the two diffracted wavetrains with the increase in the OPD.

The paper shows that by routing each beam from a low coherence two beam interferometer via separate parts of the diffraction grating in an interrogation spectrometer is possible to sense the sign of the optical path difference in the interferometer and eliminate the mirror terms in FDOCT. This is obtained here using screens to obscure halves of the two beams. The screens modify radically the operation of the system. With no screens, the system is similar to that largely used in low coherence interferometry sensing [1-5] and FDOCT [6-10], consisting of an interferometer followed by a spectrometer. When the screens are in, the behavior is similar to that encountered in an experiment of generating Talbot bands [21]. While this set-up is useful in developing a unique model for SDWLI, FDOCT and Talbot bands, it is inefficient in terms of power use. We are now devising equivalent more power efficient set-ups using optical fibers to route light along two optical paths, one for the reference and the other via the object arm and illuminating separate parts of the diffraction grating.

The model developed and the sketches in Table 1 explain the effect on the channelled spectrum visibility of introducing an OPD in the interferometer. The model could be extended to the case where the two beams cover a different number of grating lines and a gap is left on the grating between the two beams. Without writing any equations however, it is possible to infer the effect of a gap using the interpretation of delayed wavetrains in Table 1. The gap, covering M grating lines will require an OPD of at least $\pm M\lambda$ before the two wavetrains could overlap. Therefore, such a method could be used for adjustment of the minimum path imbalance, with possible applications in sensor multiplexing.

The sketches in Table 1 are applicable to any type of spectrometer, using diffraction gratings or prisms, the findings here are not restricted to spectral analysis performed by diffraction. Equivalent explanation could be produced for a spectrometer based on dispersion by writing the effect of the dispersion on the delay of different parts of the beams traversing the prism [20].

#81518 - $15.00 USD Received 29 Mar 2007; revised 17 Jul 2007; accepted 18 Jul 2007; published 20 Jul 2007